ACS APPLIED MATERIALS & INTERFACES

Research Article

www.acsami.org

Redox-Sensitive and Intrinsically Fluorescent Photoclick Hyaluronic Acid Nanogels for Traceable and Targeted Delivery of Cytochrome *c* to Breast Tumor in Mice

Shuai Li,[†] Jian Zhang,[†] Chao Deng,*[,†] Fenghua Meng,[†] Lin Yu,[‡] and Zhiyuan Zhong*[,†]

[†]Biomedical Polymers Laboratory, College of Chemistry, Chemical Engineering and Materials Science, Soochow University, Suzhou, 215123, China

[‡]State Key Laboratory of Molecular Engineering of Polymers, Fudan University, Shanghai 200433, China

Supporting Information

ABSTRACT: In spite of their high specificity and potency, few protein therapeutics are applied in clinical cancer therapy owing to a lack of safe and efficacious delivery systems. Here, we report that redox-sensitive and intrinsically fluorescent photoclick hyaluronic acid nanogels (HA-NGs) show highly efficient loading and breast tumor-targeted delivery of cytochrome *c* (CC). HA-NGs were obtained from hyaluronic acid-*graft*-oligo(ethylene glycol)-tetrazole (HA-OEG-Tet) via inverse nanoprecipitation and catalyst-free photoclick cross-linking with L-cystine dimethacrylamide (MA-Cys-MA). HA-NGs exhibited a superb CC loading content of up to 40.6 wt %, intrinsic fluorescence (λ_{em} = 510 nm), and a small size of ca. 170 nm. Notably, CC-loaded nanogels (CC-NGs) showed a fast glutathione-responsive protein release behavior. Importantly, released CC maintained its bioactivity. MTT assays revealed that CC-NGs were highly potent with a low IC_{50} of 3.07 μM to CD44+ MCF-7 human breast tumor cells. Confocal microscopy observed efficient and selective internalization of fluorescent HA-NGs into MCF-7 cells. Interestingly, HA-NGs exhibited also effective breast tumor penetration. The therapeutic results demonstrated that CC-NGs effectively inhibited the growth of MCF-7 breast tumor xenografts at a particularly low dose of 80 or 160 nmol CC equiv./kg. Moreover, CC-NGs did not cause any change in mice body weight, corroborating their low systemic side effects. Redox-sensitive and intrinsically fluorescent photoclick hyaluronic acid nanogels have appeared as a "smart" protein delivery nanoplatform enabling safe, efficacious, traceable, and targeted cancer protein therapy in vivo.

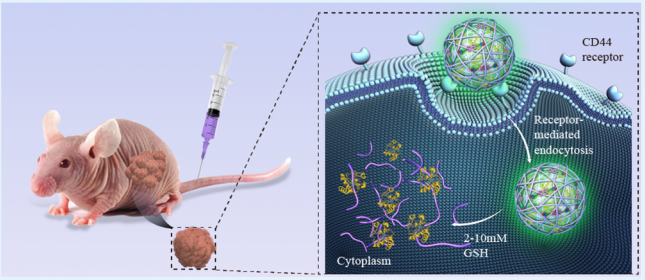

KEYWORDS: *nanogels, reduction-sensitive, click reaction, protein delivery, cancer therapy, tumor targeting*

1. INTRODUCTION

Protein therapeutics based on antibodies, cytokines, enzymes, and transcription factors have received growing interests for treatment of many diseases such as cardiovascular diseases and malignant tumors.[1−3] Unlike chemotherapeutics, protein therapeutics show generally higher specificity, better anticancer potency, and lower toxicity to healthy cells, resulting in superior clinical antitumor efficacy.[4] More than ten antibodies like trastuzumab, bevacizumab, ipilimumab, and Cetuximab are currently employed in the clinics for various oncology indications.[2] PEGylated L-asparaginase and poly(styrene-maleic acid)-conjugated neocarzinostatin are used to treat acute lymphoblastic leukemia and hepatocellular carcinoma, respectively.[5] It should be noted that clinically used protein drugs are limited to those taking effects extracellularly. Protein drugs having intracellular targets however represent a big family of protein biologics have not come to the clinics, partly due to their significantly more challenging delivery in vivo which includes not only short plasma half-life and rapid degradation but also inefficient cellular uptake and poor intracellular trafficking process.[6,7]

Various protein nanocarriers such as liposomes,[8,9] polymersomes,[10,11] nanoparticles,[12−18] and hydrogels[3] have recently been developed and explored to overcome the extracellular as well as intracellular barriers. In particular, nanogels (NGs) with excellent biocompatibility, high water content, and exceptional protein compatibility have attracted much interest for protein delivery.[19−21] Taking advantage of naturally occurring distinctive tumor microenvironment or intracellular environment, diverse stimuli-sensitive nanogels have been explored to accomplish triggered protein release at the target sites.[22,23] For example, Akiyoshi et al. developed acid-labile NGs based on cholesteryl-modified pullulan that could form complex with BSA under neutral conditions while release it at pH 4.0 on a time scale of days.[24] Kurisawa et al. reported that a ternary

Received: May 15, 2016
Accepted: August 2, 2016
Published: August 10, 2016

DOI: 10.1021/acsami.6b05775
ACS Appl. Mater. Interfaces 2016, 8, 21155−21162

Scheme 1. Illustration of Redox-Sensitive and Intrinsically Fluorescent Photoclick Hyaluronic Acid Nanogels for Highly Efficient Loading and Breast Tumor-Targeted Delivery of Cytochrome *c*

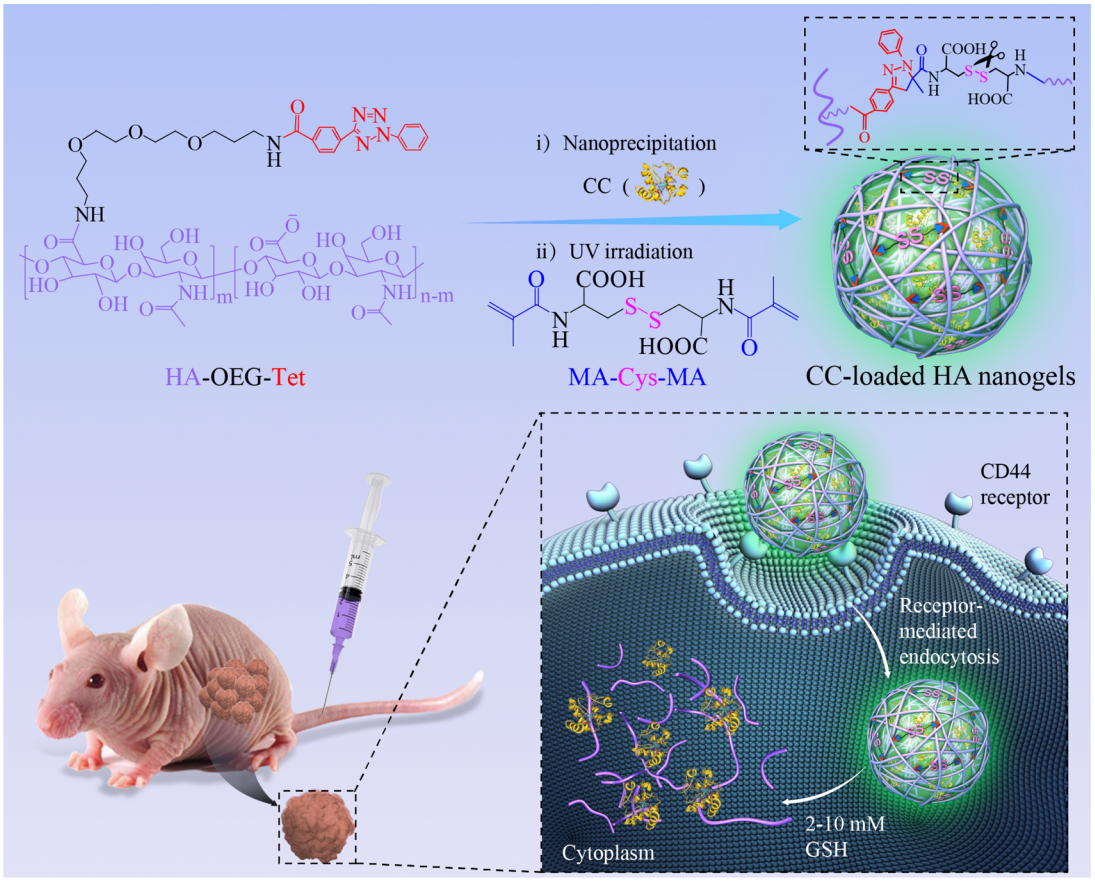

nanogel based on hyaluronic acid-green tea catechin, linear polyethylenimine, and granzyme B (GrB) achieved targeted intracellular delivery of GrB to HCT-116 cancer cells in vitro.[25] Jacob et al. reported that pH-sensitive alginate NGs prepared with adjustable pore size by microfluidics exhibited a high BSA encapsulation efficiency of over 70% and a sustained protein release profile.[26] To overcome the generally low stability of physical nanogels, chemical cross-linking methods such as radical polymerization, Michael addition reaction, copper-mediated click reaction, and amidation have been employed to prepare more stable nanogels.[27,28] For example, Thayumanavan et al. prepared pH-sensitive nanogels via radical polymerization for triggered release of α-glucosidase (a lysosomal protein) at pH 5.0.[29] Haag et al. reported that boronate cross-linked stimuli-responsive NGs based on dendritic polyglycerol could competently deliver proteins into cancer cells, achieving significant in vitro antitumor effects in MCF-7 cells.[30,31] van Nostrum et al. reported that dextran NGs following the immobilization of a model antigen (ovalbumin) via disulfide bonds could achieve triggered antigen release in dendritic cells, and boost the MHC class I antigen presentation.[32] We found that redox-sensitive NGs formed in situ could achieve easy protein encapsulation and accelerated cytoplasmic protein release.[33] However, many of these chemical nanogels suffer from nonspecific cross-linking reaction that could cause cross-reaction and denaturation of proteins. Moreover, in spite of many reports on nanogels for protein delivery, few show active tumor-targetability and efficient delivery of therapeutic proteins in vivo.

Here, we report on redox-sensitive and intrinsically fluorescent photoclick hyaluronic acid nanogels (HA-NGs) for highly efficient loading and active CD44-targeting intracellular delivery of cytochrome C (CC), a potent apoptotic protein, to xenografted breast tumor in mice (Scheme 1). HA-NGs are obtained from hyaluronic acid-*graft*-oligo(ethylene glycol)-tetrazole (HA-OEG-Tet) via inverse nanoprecipitation and "tetrazole-alkene" photoclick cross-linking with L-cystine dimethacrylamide (MA-Cys-MA). This photoclick chemistry is bioorthogonal and catalyst-free, which circumvents cross-reaction and denature of therapeutic proteins as well as potential toxic contamination.[34] HA is a natural material that shows unique targeting effect to CD44+ tumor cells like MCF-7 and MDA-MB-231cells.[35,36] MA-Cys-MA cross-linker provides HA-NGs with both high stability and reduction-sensitivity, facilitating fast protein release inside tumor cells. In addition, "tetrazole-alkene" photoclick products possess intrinsic fluorescence,[37,38] which can be employed to monitor the cellular internalization and intracellular transportation of NGs in vitro as well as tumor penetration in vivo. Notably, our results show that CC-loaded HA-NGs (CC-NGs) exhibit a high and selective antitumor effect to MCF-7 cells in vitro as well as efficient suppression of tumor growth and little systemic adverse effects in vivo.

2. EXPERIMENTAL SECTION

2.1. Synthesis of HA-OEG-Tet. HA-OEG-Tet was prepared by the amidation reaction between Tet and 4,7,10-trioxa-1,13-tridecanediamine (TTDA) followed by grafting onto HA. Tet (200 mg, 0.75

DOI: 10.1021/acsami.6b05775
ACS Appl. Mater. Interfaces 2016, 8, 21155−21162

mmol) was activated using CDI (126 mg, 0.78 mmol) for 20 min in anhydrous DMF (10 mL), and then dropwise added to TTDA (330 mg, 1.50 mmol) in anhydrous DMF (5 mL) under stirring. The reaction proceeded under nitrogen atmosphere for 2 h at ambient temperature. The DMF solution following concentration was precipitated in deionized water (10 mL) to obtain raw product. The resulting NH_2−OEG-Tet was further purified by washing with deionized water for three times. Yield: 40%. ^{1}H NMR (400 MHz, DMSO-d_6, δ, Figure S1A): 8.67 (t, 1H, —N*H*CO—), 8.25 and 8.17 (m, 4H, C_6H_4 of Tet), 8.07, 7.71, and 7.64 (m, 5H, C_6H_5 of Tet), 3.52 (m, 8H, $NH_2CH_2CH_2CH_2O(CH_2CH_2O)_2$—), 3.46 (m, 4H, $NH_2CH_2CH_2CH_2O(CH_2CH_2O)_2CH_2$—), 3.42 (m, 2H, —$CONHCH_2$—), 2.59 (t, 2H, NH_2CH_2—), 1.79 (m, 2H, —$CONHCH_2CH_2$—), 1.57 (m, 2H, $NH_2CH_2CH_2$—).

HA (140 mg, 0.004 mmol) dissolved in deionized water (5 mL) was activated with EDC (69 mg, 0.36 mmol) and NHS (21 mg, 0.18 mmol) at pH 6.0 for 30 min. Fifteen mL of DMSO and a solution of NH_2-OEG-Tet (55 mg, 0.12 mmol) in DMSO (9 mL) were added sequentially. The reaction proceeded for 24 h at 35 °C. HA-OEG-Tet product was purified by sequential dialysis (MWCO 7000) in DMSO and D.I. water and then lyophilized. Yield: 95.8%. ^{1}H NMR (400 MHz, D_2O, δ, Figure 1): OEG-Tet: 8.30−7.25 (m, 9H, —C_6H_4 and —C_6H_5 of Tet), 3.54 (m, 8H, —$NHCH_2CH_2CH_2O$-$(CH_2CH_2O)_2$—), 3.08 (m, 8H, (—$NHCH_2CH_2CH_2O$-$(CH_2CH_2O)_2$), 1.61 (m, 4H, —$CONHCH_2CH_2$—); HA: 4.50−3.67, 3.44−3.34, and 1.97. DS was calculated from peaks at δ 8.30−7.25 (phenyl protons in Tet) and δ 4.60−4.30 (anomeric proton in HA).

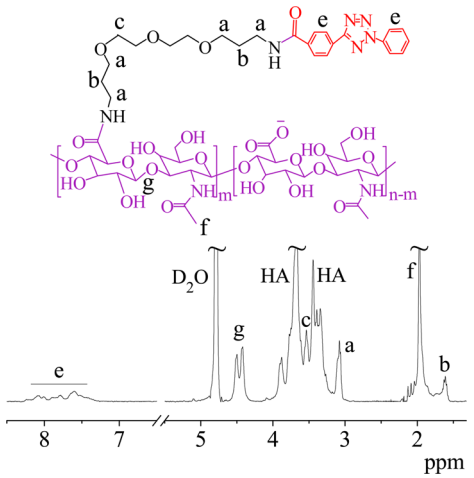

Figure 1. ^{1}H NMR (400 MHz, D_2O) of HA-OEG-Tet.

2.2. Synthesis of MA-Cys-MA. Cys (1.2 g, 5.0 mmol) in NaOH (1.5 M, 10 mL) was slowly added to MAC (2.0 mL, 20.6 mmol) in DCM (10 mL) at 0 °C. The reaction was conducted at a constant pH of 9.0 and 0 °C for 4 h. The aqueous phase was separated and precipitated using 3.0 mL of HCl (2 M). The product was obtained by filtration and drying in vacuo. Yield: 90%. ^{1}H NMR (400 MHz, DMSO-d_6, δ, Figure S1B): 12.92 (s, 2H, —COO*H*), 8.24 (d, 2H, —CON*H*—), 5.72 and 5.39 (d, 4H, CH_2=$C(CH_3)$—), 4.53 (m, 2H, —NHC*H*(COOH)CH_2—), 3.18 and 3.03 (m, 4 H, —CH_2SS—), 1.85 (s, 6H, -CH_3).

2.3. Preparation and Reduction-Responsivity of Fluorescent HA-NGs. HA-NGs were prepared from HA-OEG-Tet by inverse nanoprecipitation and then catalyst-free "tetrazole-alkene" photoclick cross-linking in the presence of MA-Cys-MA at a Tet/MA molar ratio of 1. Typically, 1 mL of HA-OEG-Tet (1 mg/mL) and MA-Cys-MA solution in PB (10 mM, pH 8.5) was added to acetone (20 mL). The resulting dispersion was irradiated with UV (320−390 nm, 37.5 mW/cm^2) for 90 s followed by the evaporation of acetone solvent to obtain HA-NG dispersion in water. HA-NGs were obtained by massive dialysis (MWCO 7000 Da) in PB for 12 h, and freeze-drying. Autofluorescence of the NG suspension in PB following the excitation with portable UV lamp (302 nm) was recorded using a Nikon Digital camera. The reduction-responsivity of HA-NGs was examined by monitoring the size change of NGs at 37 °C under shaking at 200 rpm with 10 mM GSH by DLS.

2.4. Encapsulation and Release of CC. CC-loaded HA NGs (CC-NGs) were obtained similarly as the formation of blank HA-NGs except that a certain amount of CC (theoretical loading contents ranging from 30%, 40%, to 50%) was added into the aqueous solution of HA-OEG-Tet and MA-Cys-MA in PB (10 mM, pH 8.5) before injecting into acetone. To calculate protein loading content (PLC) and protein loading efficiency (PLE), lyophilized CC-NGs were dissolved in PB with GSH (10 mM) to disrupt cross-linked structure and release CC. The amount of CC was determined using UV−vis spectrometry based on a calibration curve established with known concentrations of CC. PLC and PLE were calculated according to the following formula:

$$\text{PLC (wt.\%)} = (\text{weight of loaded protein} / \text{total weight of polymer and protein}) \times 100$$

$$\text{PLE} = (\text{weight of loaded protein} / \text{weight of protein in feed}) \times 100$$

The release studies were conducted in triplicate at 37 °C and pH 7.4 in PB or PB with 10 mM GSH. Typically, 1.0 mL of CC-NG solution (0.7 mg/mL) in a dialysis tube (MWCO 350 kDa) was dialyzed in 20 mL of release media to acquire sink conditions under shaking at 37 °C. Five mL of released media was withdrawn at predetermined time, and refilled with 5 mL of new medium. CC amount was measured using UV−vis spectrophotometer with a peak at 410 nm.

2.5. In Vivo Antitumor Efficacy. Subcutaneous human breast tumor xenografts were obtained by inoculating MCF-7 tumor block (1.0 mm^3/mouse) subcutaneously to female nude mice at the left flank. All mice were housed in Laboratory Animal Center of Soochow University and were handled under protocols approved by the Animal Care and Use Committee of Soochow University. After 7 days, the tumor size reached 30−60 mm^2, and mice were randomly divided into 4 groups and administered via the intravenous injection of CC-NGs, free CC, and PBS, respectively. Drugs were administered every other day for five times. Tumor growth was monitored every other day, and the tumor volume was determined as $(L \times W \times H)/2$, in which L, W, and H are the tumor longest, widest, and highest direction, respectively. Mice were weighed and normalized to their initial weights.

3. RESULTS AND DISCUSSION

3.1. Synthesis of HA-OEG-Tet and MA-Cys-MA. HA-OEG-Tet was readily obtained by grafting NH_2-OEG-Tet onto HA (Scheme 2). NH_2-OEG-Tet was prepared by the amidation reaction between TTDA and Tet in the presence of CDI (Scheme S1A of the Supporting Information). The incorporation of OEG could improve graft efficiency and increase the water solubility of HA-Tet conjugates, facilitating preparation of nanogels with a high cross-linking density. ^{1}H NMR spectrum of NH_2-OEG-Tet showed clear signals attributed to Tet (δ 8.67, 8.25, 8.17, 8.07, 7.71, and 7.64) and TTDA moieties (δ 3.52, 3.46, 3.42, 2.59, 1.79, and 1.57) (Figure S1A). The integral ratio of signals at δ 8.25−8.17 (phenyl protons of Tet) and δ 1.57 (methylene protons of TTDA) was close to 1:1, confirming equivalent coupling of Tet to TTDA. NH_2-OEG-Tet was conjugated to HA in a mixed solvent of water and DMSO through EDC/NHS coupling reaction. ^{1}H NMR spectrum displayed besides resonances attributable to HA backbone (δ 4.50−3.67, 3.44−3.34, 1.97) also characteristic signals of NH_2-OEG-Tet moiety (δ 8.30−7.25, 3.54, 3.08, and 1.61) (Figure 1). The DS of HA-OEG-Tet might be calculated from the peaks at δ 8.30−7.25 assignable to Tet and δ 4.60−

DOI: 10.1021/acsami.6b05775
ACS Appl. Mater. Interfaces 2016, 8, 21155−21162

Scheme 2. Synthesis of HA-OEG-Tet. Condition: EDC/NHS, DMSO/H_2O, 35 °C, 24 h

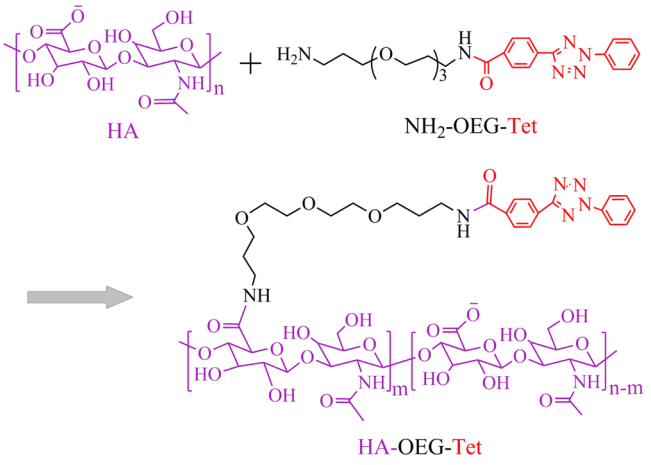

4.30 due to HA. Herewith, HA-OEG-Tet adducts with distinct DS of 4.6, 6.5, and 8.5 were obtained at HA carboxyl group/NH_2-OEG-Tet molar feeding ratios of 4/1, 3/1, and 2/1, respectively (Table S1). The water solubility of HA-OEG-Tet conjugates was highly dependent on their DS, in which HA-OEG-Tet with DS of 4.6 and 6.5 displayed good water solubility while HA-OEG-Tet at a high DS of 8.5 could not readily be dissolved in water. In order to achieve high cross-linking density, HA-OEG-Tet with DS 6.5 was selected for nanogel formation.

MA-Cys-MA was readily obtained with a high yield of 90% by the amidation reaction between Cys and MAC (Scheme S1B) as reported for L-cystine bis(acrylamide).[39] ^{1}H NMR spectrum of MA-Cys-MA showed clearly characteristic signals of both MA (δ 5.72, 5.39 and 1.85) and Cys (δ 12.92, 8.24, 4.53, 3.18 and 3.03) (Figure S1B). The peaks at δ 4.53 (methine proton of Cys) and δ 1.84 (methyl proton of MA) exhibited an intensity ratio near to 1:3, corroborating successful synthesis of MA-Cys-MA.

3.2. Formation and Characterization of HA-NGs. HA-NGs were prepared by dropwise adding an aqueous solution of HA-OEG-Tet and MA-Cys-MA into acetone, followed by UV irradiation for 90 s. The photoclick cross-linking reaction between tetrazole groups of HA-OEG-Tet and methacrylate groups of MA-Cys-MA was followed with UV. The results displayed that the absorbance at 275 nm attributed to tetrazole groups completely disappeared after UV irradiation (Figure 2A), confirming that the cross-linking reaction for NG formation was fast and quantitative. DLS measurements showed that HA-NGs had a mean diameter of 165 nm and a polydispersity (PDI) of 0.20 (Figure 2B). TEM displayed that HA-NGs were spherical and had a small size of ca. 100 nm (Figure 2B). HA-NGs exhibited a negative surface charge of −20.0 mV (Table 1), which derives from the HA carboxyl groups on the surface as observed for other HA nanoparticles.[40,41] Interestingly, these NGs exhibited strong intrinsic fluorescence with an emission wavelength of 510 nm (Figure 2C), which provides a tool for the facile observation of cellular uptake, intracellular trafficking, and tumor penetration of NGs. It should be noted that HA-NGs displayed excellent stability with little size change against 100-fold dilution (Figure 2D), while significant aggregation and dissociation under 10 mM glutathione (GSH) at 24 h due to cleavage of disulfide bonds, supporting that HA-NGs are reduction-sensitive.

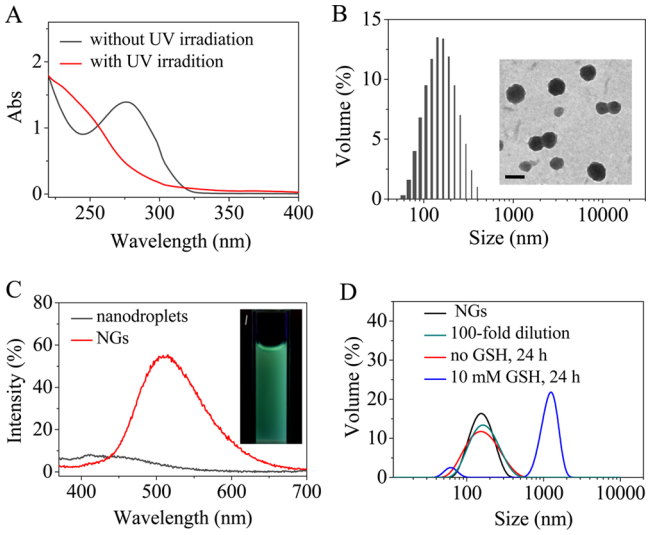

Figure 2. Characterization of HA-NGs. (A) UV absorption spectra of HA nanodroplets with and without UV irradiation. The absorption peak at 275 nm derives from tetrazole groups; (B) size and size distribution of HA-NGs measured by DLS and TEM. The scale bar in TEM micrograph represents 100 nm; (C) fluorescence emission spectra of HA nanodroplets and HA-NGs (λ_{ex} = 350 nm). The inset showed the fluorescence image of HA-NGs; (D) change of size distribution of HA-NGs against dilution or 10 mM GSH at 37 °C.

3.3. Encapsulation and Release of CC. The protein loading experiments showed that CC could be easily loaded into HA-NGs at theoretical loading contents ranging from 30 to 50 wt %. A remarkably high encapsulation content of 40.6 wt % was obtained (Table 1), likely resulting from electrostatic and hydrophobic interactions between CC and HA. This high protein loading of HA-NGs would significantly reduce injection volume and use of nanocarrier materials, renders them superior to many reported protein delivery systems.[42−44] DLS measurement showed that HA-NGs following CC encapsulation displayed a small size of around 170 nm, a narrow PDI, and a negative zeta potential of about −15 mV. The negative zeta potential of CC-NGs suggests that CC is loaded inside of the NGs, which on the one hand protects CC from degradation and on the other hand provides excellent colloidal stability.[45]

Interestingly, CC release from HA-NGs was largely inhibited at pH 7.4 and 37 °C (Figure 3A), in which less than 20% CC was released in 24 h. On the contrary, 54.7% and 84.6% CC were released from NGs in 6 and 24 h under a reductive condition (10 mM GSH), indicating that protein release can be triggered under cytoplasmic reductive environment. The cytosol of tumor cells has a high GSH concentration of ca. 2−10 mM.[46] More importantly, ABTS assays displayed that CC released from NGs had a similar catalytic activity to native CC (Figure 3B), supporting that proteins following the whole process of encapsulation, photoclick cross-linking, and in vitro release still maintain their enzymatic bioactivity.

3.4. Targetability and Anti-Tumor Activity of CC-NGs toward CD44+ MCF-7 Cells. MTT assays showed that the cell viability of MCF-7 and U87 cells treated with blank HA-NGs for 48 h at a tested concentration up to 1.0 mg/mL was close to 100% (Figure 4A), supporting that HA-NGs are nontoxic and possess good biocompatibility. The in vitro antitumor studies in MCF-7 cells possessing high CD44 expression revealed that CC-NGs had a remarkable antitumor effect with a low IC_{50} of 3.07 μM, while free CC caused little

DOI: 10.1021/acsami.6b05775
ACS Appl. Mater. Interfaces 2016, 8, 21155−21162

Table 1. Characteristics of HA-NGs and CC-NGs

entry	PLC (wt %) theory	PLC (wt %) determined[a]	PLE[a] (%)	size[b] (nm)	PDI[b]	Zeta[c] (mV)
1	0			165	0.20	−20.0
2	30	24.9	77.0	170	0.20	−14.7
3	40	33.2	74.6	171	0.17	−14.0
4	50	40.6	68.4	174	0.17	−13.8

[a]Determined by UV−vis absorption of CC at 410 nm in water. [b]Measured with DLS at 25 °C in PB. [c]Measured with Zetasizer Nano-ZS at 25 °C.

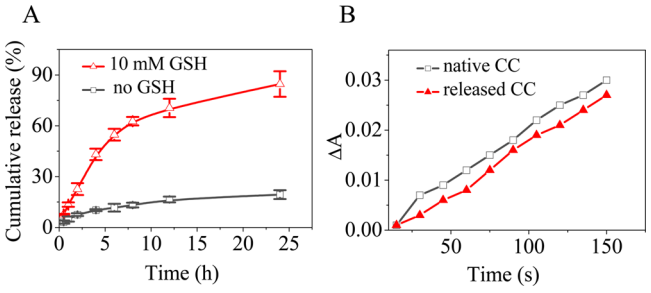

Figure 3. (A) The cumulative release of CC from CC-NGs at 37 °C in 10 mM PB with or without 10 mM GSH and (B) oxidation of ABTS with native or released CC (4.0 μg/mL).

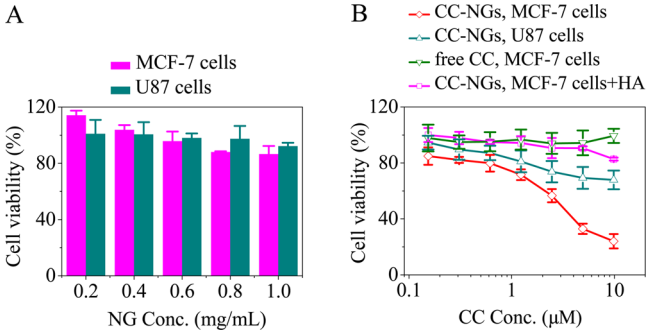

Figure 4. MTT assays of HA-NGs and CC-NGs in MCF-7 and U87 cells. (A) Cytotoxicity of HA-NGs. The cells were incubated with NGs for 48 h; and (B) antitumor activity of free CC and CC-NGs. Data are shown as mean ± SD (n = 4).

antitumor effect with cell viability higher than 90% even at a high protein concentration of 10.24 μM likely due to poor cell internalization (Figure 4B). As expected, CC-NGs displayed significantly reduced apoptotic activity in U87 cancer cells possessing low CD44 expression, wherein ca. 68% cell viability was detected at 10.24 μM CC after 72 h incubation. The antitumor effect of CC-NGs to MCF 7 cells was greatly decreased by priming the cells with free HA, validating receptor-mediated uptake of HA-NGs.

Taking advantage of their autofluorescence, cellular internalization and intracellular trafficking of HA-NGs can be conveniently monitored using CLSM. The confocal images revealed obvious NG fluorescence in the cytosol of MCF-7 cells after 2 h treatment, and the fluorescence intensity significantly increased at 4 h (Figure 5), corroborating efficient uptake of HA-NGs by MCF-7 cells. On the contrary, negligible nanogel fluorescence is observed in U87 cells under otherwise the same conditions. Moreover, pretreating MCF-7 cells with free HA before incubation with HA-NGs significantly reduced intracellular NG fluorescence. It is evident, therefore, that HA-NGs can actively target CD44-positive cancer cells as previous reports for other HA nanoparticles.[47−51]

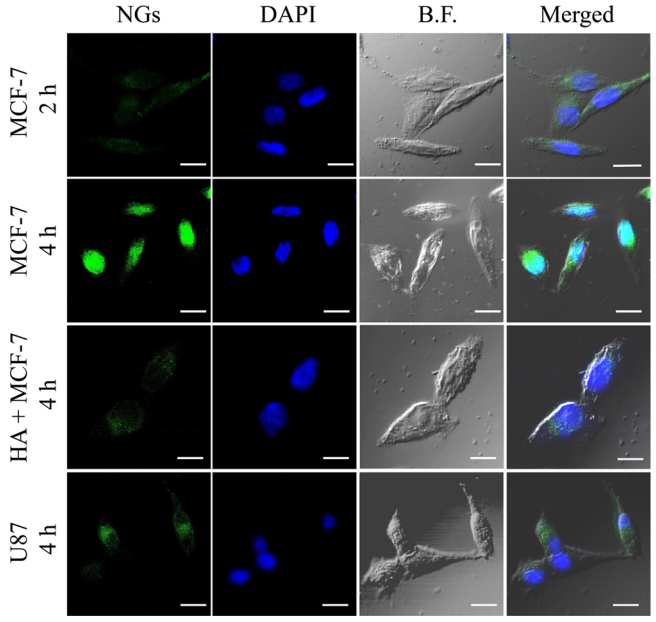

Figure 5. CLSM images of MCF-7 and U87 cancer cells after incubation with 0.8 mg/mL blank HA-NGs (scale bar =20 μm).

3.5. In Vivo Tumor Penetration and Therapeutic Efficacy. The penetration and distribution of nanomedicines in the tumor is a critical factor for achieving effective tumor therapy.[52−54] Here, the autofluorescence of HA-NGs was employed to observe tumor penetration of NGs in xenografted MCF-7 breast tumor in mice. The CLSM images of MCF-7 tumor sections showed that most of HA-NGs (green fluorescence) colocalized with blood vessels (red fluorescence) at 1 h post injection (Figure 6). With the time extended to 6 h, the NGs moved away from the blood vessels and mainly located at the vicinity of blood vessels. Notably, HA-NGs spread all over the whole tumor at 24 h post injection, corroborating that they possess exceptional tumor penetration ability in human MCF-7 tumor xenografts.

The antitumor effect of CC-NGs was investigated in MCF-7 tumor-bearing mice. The mice with tumor volume of about 30−60 mm^3 were treated by intravenous injection of CC-NGs at a dosage of 80 or 160 nmol CC equiv./kg. As expected, mice administrated with PBS and free CC controls displayed rapid tumor progression with relative tumor size on day 16 reached 52 and 44, respectively (Figure 7A). The slight difference of tumor sizes between PBS and free CC groups indicated that direct administration of therapeutic proteins results in very limited antitumor effect possibly due to their rapid degradation in vivo, inefficient cellular uptake and poor intracellular trafficking process. In contrast, tumor growth was significantly inhibited by CC-NGs at both 80 and 160 nmol CC equiv./kg (Figure 7A). The higher protein dosage resulted in obviously

DOI: 10.1021/acsami.6b05775
ACS Appl. Mater. Interfaces 2016, 8, 21155−21162

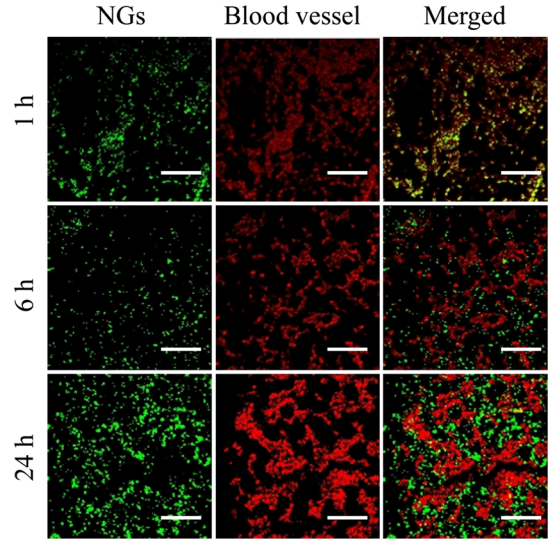

Figure 6. Immunofluorescence staining of tumor at 1 h, 6 h and 24 h postinjection of HA-NGs. The red and green fluorescences indicate the tumor blood vessels and HA-NGs, respectively (scale bar =50 μm).

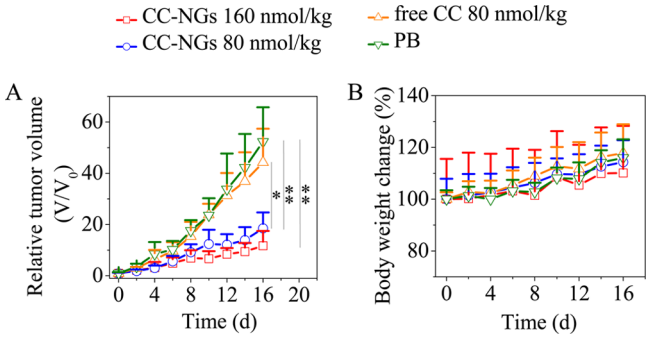

Figure 7. In vivo antitumor performance of CC-NGs in MCF-7 tumor xenografts. (A) Relative tumor volume of mice administrated with CC-NGs, free CC or PBS. Injection was scheduled on day 0, 2, 4, 6, and 8 at a dosage of 80 or 160 nmol CC equiv./kg. *p < 0.05, **p < 0.01 (Student's t test); and (B) mice body weight changes following different treatments in 16 d. Data are presented as mean ± SD (n = 5).

better tumor regression. Notably, mice treated with CC-NGs, as for those with PBS, displayed no body weight loss (Figure 7B), indicating that CC-NGs have little systemic toxicity. Thus, CC-NGs with high stability, active tumor-targetability, and triggered intracellular release exhibited efficacious cancer protein therapy with minimal adverse effects. It is reasonable to deduce that HA-NGs can be employed as a decent nanoplatform for the tumor-targeted delivery of more potently intracellular protein therapeutics like GrB, apoptin, and TRAIL.[55−58]

4. CONCLUSIONS

We have shown that redox-sensitive and intrinsically fluorescent hyaluronic acid nanogels (HA-NGs) exhibited highly efficient loading and targeted delivery of cytochrome C (CC) to xenografted MCF-7 breast tumor in mice. The resulting HA-NGs have several unique properties: (i) they are formed via "tetrazole-alkene" photoclick reaction that not only possesses a great specificity, but also avoids use of any toxic catalysts, fully maintaining protein bioactivity and circumventing potential toxic contamination; (ii) they exhibit a superb CC loading content of up to 40.6 wt %; (iii) they can actively target to and be efficiently internalized by cancer cells with high CD44 receptor expression; (iv) they can rapidly release therapeutic proteins under the cytoplasmic reductive condition, providing potent antitumor effect in CD44+ cancer cells in vitro and in vivo; (v) they display intrinsic fluorescence that can be employed to monitor their cellular uptake in vitro and tumor penetration in vivo. These redox-sensitive and intrinsically fluorescent photoclick HA-NGs have emerged as a multifunctional and potentially viable nanoplatform for traceable and targeted protein delivery.

■ ASSOCIATED CONTENT

Supporting Information

The Supporting Information is available free of charge on the ACS Publications website at DOI: 10.1021/acsami.6b05775.

Experimental on materials, characterization, detection of enzymatic activity of CC released from HA-NGs, cellular uptake of fluorescent HA-NGs, MTT assays, and immunofluorescent analysis for tumor penetration; synthesis scheme and ^{1}H NMR spectra for NH_2-OEG-Tet and MA-Cys-MA; and synthesis results for HA-OEG-Tet (PDF)

■ AUTHOR INFORMATION

Corresponding Authors

*Tel: +86-512-65884933; e-mail: cdeng@suda.edu.cn (C.D.).
*Tel: +86-512-65880098; e-mail: zyzhong@suda.edu.cn (Z.Z.).

Notes

The authors declare no competing financial interest.

■ ACKNOWLEDGMENTS

This work was supported by the National Natural Science Foundation of China (NSFC 51273137, 51473110, 51403147 and 51225302).

■ REFERENCES

(1) Walsh, G. Biopharmaceutical Benchmarks 2014. *Nat. Biotechnol.* **2014**, *32*, 992−1000.
(2) Sliwkowski, M. X.; Mellman, I. Antibody Therapeutics in Cancer. *Science* **2013**, *341*, 1192−1198.
(3) Vermonden, T.; Censi, R.; Hennink, W. E. Hydrogels for Protein Delivery. *Chem. Rev.* **2012**, *112*, 2853−2888.
(4) Leader, B.; Baca, Q. J.; Golan, D. E. Protein Therapeutics: A Summary and Pharmacological Classification. *Nat. Rev. Drug Discovery* **2008**, *7*, 21−39.
(5) Duncan, R. Polymer Conjugates as Anticancer Nanomedicines. *Nat. Rev. Cancer* **2006**, *6*, 688−701.
(6) Pisal, D. S.; Kosloski, M. P.; Balu-Iyer, S. V. Delivery of Therapeutic Proteins. *J. Pharm. Sci.* **2010**, *99*, 2557−2575.
(7) Gu, Z.; Biswas, A.; Zhao, M.; Tang, Y. Tailoring Nanocarriers for Intracellular Protein Delivery. *Chem. Soc. Rev.* **2011**, *40*, 3638−3655.
(8) Sarker, S. R.; Hokama, R.; Takeoka, S. Intracellular Delivery of Universal Proteins Using a Lysine Headgroup Containing Cationic Liposomes: Deciphering the Uptake Mechanism. *Mol. Pharmaceutics* **2014**, *11*, 164−174.
(9) Yuba, E.; Harada, A.; Sakanishi, Y.; Watarai, S.; Kono, K. A Liposome-Based Antigen Delivery System Using pH-Sensitive Fusogenic Polymers for Cancer Immunotherapy. *Biomaterials* **2013**, *34*, 3042−3052.
(10) Lu, L.; Zou, Y.; Yang, W.; Meng, F.; Deng, C.; Cheng, R.; Zhong, Z. Anisamide-Decorated pH-Sensitive Degradable Chimaeric Polymersomes Mediate Potent and Targeted Protein Delivery to Lung Cancer Cells. *Biomacromolecules* **2015**, *16*, 1726−1735.

DOI: 10.1021/acsami.6b05775
ACS Appl. Mater. Interfaces 2016, 8, 21155−21162

(11) Sun, H.; Meng, F.; Cheng, R.; Deng, C.; Zhong, Z. Reduction and pH Dual-Bioresponsive Crosslinked Polymersomes for Efficient Intracellular Delivery of Proteins and Potent Induction of Cancer Cell Apoptosis. *Acta Biomater.* **2014**, *10*, 2159−2168.
(12) Danhier, F.; Ansorena, E.; Silva, J. M.; Coco, R.; Le Breton, A.; Preat, V. PLGA-Based Nanoparticles: An Overview of Biomedical Applications. *J. Controlled Release* **2012**, *161*, 505−522.
(13) Wu, J.; Kamaly, N.; Shi, J.; Zhao, L.; Xiao, Z.; Hollett, G.; John, R.; Ray, S.; Xu, X.; Zhang, X.; Kantoff, P. W.; Farokhzad, O. C. Development of Multinuclear Polymeric Nanoparticles as Robust Protein Nanocarriers. *Angew. Chem., Int. Ed.* **2014**, *53*, 8975−8979.
(14) Chung, J. E.; Tan, S.; Gao, S. J.; Yongvongsoontorn, N.; Kim, S. H.; Lee, J. H.; Choi, H. S.; Yano, H.; Zhuo, L.; Kurisawa, M.; Ying, J. Y. Self-Assembled Micellar Nanocomplexes Comprising Green Tea Catechin Derivatives and Protein Drugs for Cancer Therapy. *Nat. Nanotechnol.* **2014**, *9*, 907−912.
(15) Kim, S. K.; Foote, M. B.; Huang, L. The Targeted Intracellular Delivery of Cytochrome C Protein to Tumors Using Lipid-Apolipoprotein Nanoparticles. *Biomaterials* **2012**, *33*, 3959−3966.
(16) Wang, M.; Alberti, K.; Sun, S.; Arellano, C. L.; Xu, Q. Combinatorially Designed Lipid-Like Nanoparticles for Intracellular Delivery of Cytotoxic Protein for Cancer Therapy. *Angew. Chem., Int. Ed.* **2014**, *53*, 2893−2898.
(17) Minardi, S.; Pandolfi, L.; Taraballi, F.; De Rosa, E.; Yazdi, I. K.; Liu, X.; Ferrari, M.; Tasciotti, E. PLGA-Mesoporous Silicon Microspheres for the in Vivo Controlled Temporospatial Delivery of Proteins. *ACS Appl. Mater. Interfaces* **2015**, *7*, 16364−16373.
(18) Lee, B. R.; Oh, K. T.; Oh, Y. T.; Baik, H. J.; Park, S. Y.; Youn, Y. S.; Lee, E. S. A Novel pH-Responsive Polysaccharidic Ionic Complex for Proapoptotic D-(KLAKLAK)(2) Peptide Delivery. *Chem. Commun.* **2011**, *47*, 3852−3854.
(19) Zhang, X.; Malhotra, S.; Molina, M.; Haag, R. Micro- and Nanogels with Labile Crosslinks - from Synthesis to Biomedical Applications. *Chem. Soc. Rev.* **2015**, *44*, 1948−1973.
(20) Tahara, Y.; Akiyoshi, K. Current Advances in Self-Assembled Nanogel Delivery Systems for Immunotherapy. *Adv. Drug Delivery Rev.* **2015**, *95*, 65−76.
(21) Li, Y.; Maciel, D.; Rodrigues, J.; Shi, X.; Tomas, H. Biodegradable Polymer Nanogels for Drug/Nucleic Acid Delivery. *Chem. Rev.* **2015**, *115*, 8564−8608.
(22) Lu, Y.; Sun, W.; Gu, Z. Stimuli-Responsive Nanomaterials for Therapeutic Protein Delivery. *J. Controlled Release* **2014**, *194*, 1−19.
(23) Cheng, R.; Meng, F.; Deng, C.; Zhong, Z. Bioresponsive Polymeric Nanotherapeutics for Targeted Cancer Chemotherapy. *Nano Today* **2015**, *10*, 656−670.
(24) Morimoto, N.; Hirano, S.; Takahashi, H.; Loethen, S.; Thompson, D. H.; Akiyoshi, K. Self-Assembled pH-Sensitive Cholesteryl Pullulan Nanogel as a Protein Delivery Vehicle. *Biomacromolecules* **2013**, *14*, 56−63.
(25) Liang, K.; Ng, S.; Lee, F.; Lim, J.; Chung, J. E.; Lee, S. S.; Kurisawa, M. Targeted Intracellular Protein Delivery Based on Hyaluronic Acid-Green Tea Catechin Nanogels. *Acta Biomater.* **2016**, *33*, 142−52.
(26) Bazban-Shotorbani, S.; Dashtimoghadam, E.; Karkhaneh, A.; Hasani-Sadrabadi, M. M.; Jacob, K. I. Microfluidic Directed Synthesis of Alginate Nanogels with Tunable Pore Size for Efficient Protein Delivery. *Langmuir* **2016**, *32*, 4996.
(27) Oh, J. K.; Drumright, R.; Siegwart, D. J.; Matyjaszewski, K. The Development of Microgels/Nanogels for Drug Delivery Applications. *Prog. Polym. Sci.* **2008**, *33*, 448−477.
(28) Jiang, Y.; Chen, J.; Deng, C.; Suuronen, E. J.; Zhong, Z. Click Hydrogels, Microgels and Nanogels: Emerging Platforms for Drug Delivery and Tissue Engineering. *Biomaterials* **2014**, *35*, 4969−4985.
(29) Molla, M. R.; Marcinko, T.; Prasad, P.; Deming, D.; Garman, S. C.; Thayumanavan, S. Unlocking a Caged Lysosomal Protein from a Polymeric Nanogel with a pH Trigger. *Biomacromolecules* **2014**, *15*, 4046−4053.
(30) Zhang, X.; Zhang, K.; Haag, R. Multi-Stage, Charge Conversional, Stimuli-Responsive Nanogels for Therapeutic Protein Delivery. *Biomater. Sci.* **2015**, *3*, 1487−1496.
(31) Steinhilber, D.; Witting, M.; Zhang, X.; Staegemann, M.; Paulus, F.; Friess, W.; Kuechler, S.; Haag, R. Surfactant Free Preparation of Biodegradable Dendritic Polyglycerol Nanogels by Inverse Nanoprecipitation for Encapsulation and Release of Pharmaceutical Biomacromolecules. *J. Controlled Release* **2013**, *169*, 289−295.
(32) Li, D.; Kordalivand, N.; Fransen, M. F.; Ossendorp, F.; Raemdonck, K.; Vermonden, T.; Hennink, W. E.; van Nostrum, C. F. Reduction-Sensitive Dextran Nanogels Aimed for Intracellular Delivery of Antigens. *Adv. Funct. Mater.* **2015**, *25*, 2993−3003.
(33) Chen, W.; Zheng, M.; Meng, F.; Cheng, R.; Deng, C.; Feijen, J.; Zhong, Z. In Situ Forming Reduction-Sensitive Degradable Nanogels for Facile Loading and Triggered Intracellular Release of Proteins. *Biomacromolecules* **2013**, *14*, 1214−1222.
(34) Ramil, C. P.; Lin, Q. Bioorthogonal Chemistry: Strategies and Recent Developments. *Chem. Commun.* **2013**, *49*, 11007−11022.
(35) Rao, N. V.; Yoon, H. Y.; Han, H. S.; Ko, H.; Son, S.; Lee, M.; Lee, H.; Jo, D.-G.; Kang, Y. M.; Park, J. H. Recent Developments in Hyaluronic Acid-Based Nanomedicine for Targeted Cancer Treatment. *Expert Opin. Drug Delivery* **2016**, *13*, 239−252.
(36) Oh, E. J.; Park, K.; Kim, K. S.; Kim, J.; Yang, J.-A.; Kong, J.-H.; Lee, M. Y.; Hoffman, A. S.; Hahn, S. K. Target Specific and Long-Acting Delivery of Protein, Peptide, and Nucleotide Therapeutics Using Hyaluronic Acid Derivatives. *J. Controlled Release* **2010**, *141*, 2−12.
(37) Song, W.; Wang, Y.; Qu, J.; Madden, M. M.; Lin, Q. A Photoinducible 1,3-Dipolar Cycloaddition Reaction for Rapid, Selective Modification of Tetrazole-Containing Proteins. *Angew. Chem., Int. Ed.* **2008**, *47*, 2832−2835.
(38) Fan, Y.; Deng, C.; Cheng, R.; Meng, F.; Zhong, Z. In Situ Forming Hydrogels Via Catalyst-Free and Bioorthogonal "Tetrazole-Alkene" Photo-Click Chemistry. *Biomacromolecules* **2013**, *14*, 2814−2821.
(39) Emilitri, E.; Ranucci, E.; Ferruti, P. New Poly(Amidoamine)S Containing Disulfide Linkages in Their Main Chain. *J. Polym. Sci., Part A: Polym. Chem.* **2005**, *43*, 1404−1416.
(40) Zhong, Y.; Goltsche, K.; Cheng, L.; Xie, F.; Meng, F.; Deng, C.; Zhong, Z.; Haag, R. Hyaluronic Acid-Shelled Acid-Activatable Paclitaxel Prodrug Micelles Effectively Target and Treat CD44-Overexpressing Human Breast Tumor Xenografts in Vivo. *Biomaterials* **2016**, *84*, 250−261.
(41) Zhao, Q.; Geng, H.; Wang, Y.; Gao, Y.; Huang, J.; Wang, Y.; Zhang, J.; Wang, S. Hyaluronic Acid Oligosaccharide Modified Redox-Responsive Mesoporous Silica Nanoparticles for Targeted Drug Delivery. *ACS Appl. Mater. Interfaces* **2014**, *6*, 20290−20299.
(42) Wu, X.; He, C.; Wu, Y.; Chen, X.; Cheng, J. Nanogel-Incorporated Physical and Chemical Hybrid Gels for Highly Effective Chemo-Protein Combination Therapy. *Adv. Funct. Mater.* **2015**, *25*, 6744−6755.
(43) Wu, C.; Boettcher, C.; Haag, R. Enzymatically Crosslinked Dendritic Polyglycerol Nanogels for Encapsulation of Catalytically Active Proteins. *Soft Matter* **2015**, *11*, 972−980.
(44) Kazazi-Hyseni, F.; van Vuuren, S. H.; van der Giezen, D. M.; Pieters, E. H.; Ramazani, F.; Rodriguez, S.; Veldhuis, G. J.; Goldschmeding, R.; van Nostrum, C. F.; Hennink, W. E.; Kok, R. J. Release and Pharmacokinetics of near-Infrared Labeled Albumin from Monodisperse Poly(D,L-Lactic-Co-Hydroxymethyl Glycolic Acid) Microspheres after Subcapsular Renal Injection. *Acta Biomater.* **2015**, *22*, 141−154.
(45) Hirsch, V.; Kinnear, C.; Moniatte, M.; Rothen-Rutishauser, B.; Clift, M. J. D.; Fink, A. Surface Charge of Polymer Coated Spions Influences the Serum Protein Adsorption, Colloidal Stability and Subsequent Cell Interaction in Vitro. *Nanoscale* **2013**, *5*, 3723−3732.
(46) Cheng, R.; Feng, F.; Meng, F.; Deng, C.; Feijen, J.; Zhong, Z. Glutathione-Responsive Nano-Vehicles as a Promising Platform for Targeted Intracellular Drug and Gene Delivery. *J. Controlled Release* **2011**, *152*, 2−12.

DOI: 10.1021/acsami.6b05775
ACS Appl. Mater. Interfaces 2016, 8, 21155−21162

(47) Li, J.; Huo, M.; Wang, J.; Zhou, J.; Mohammad, J. M.; Zhang, Y.; Zhu, Q.; Waddad, A. Y.; Zhang, Q. Redox-Sensitive Micelles Self-Assembled from Amphiphilic Hyaluronic Acid-Deoxycholic Acid Conjugates for Targeted Intracellular Delivery of Paclitaxel. *Biomaterials* **2012**, *33*, 2310−2320.
(48) Yang, J.-A.; Kong, W. H.; Sung, D. K.; Kim, H.; Kim, T. H.; Lee, K. C.; Hahn, S. K. Hyaluronic Acid-Tumor Necrosis Factor-Related Apoptosis-Inducing Ligand Conjugate for Targeted Treatment of Liver Fibrosis. *Acta Biomater.* **2015**, *12*, 174−182.
(49) Zhong, Y.; Zhang, J.; Cheng, R.; Deng, C.; Meng, F.; Xie, F.; Zhong, Z. Reversibly Crosslinked Hyaluronic Acid Nanoparticles for Active Targeting and Intelligent Delivery of Doxorubicin to Drug Resistant CD44+ Human Breast Tumor Xenografts. *J. Controlled Release* **2015**, *205*, 144−154.
(50) Yang, C.; Wang, X.; Yao, X.; Zhang, Y.; Wu, W.; Jiang, X. Hyaluronic Acid Nanogels with Enzyme-Sensitive Cross-Linking Group for Drug Delivery. *J. Controlled Release* **2015**, *205*, 206−217.
(51) Luo, Y.; Cai, X.; Li, H.; Lin, Y.; Du, D. Hyaluronic Acid-Modified Multifunctional Q-Graphene for Targeted Killing of Drug-Resistant Lung Cancer Cells. *ACS Appl. Mater. Interfaces* **2016**, *8*, 4048−4055.
(52) Prabhakar, U.; Maeda, H.; Jain, R. K.; Sevick-Muraca, E. M.; Zamboni, W.; Farokhzad, O. C.; Barry, S. T.; Gabizon, A.; Grodzinski, P.; Blakey, D. C. Challenges and Key Considerations of the Enhanced Permeability and Retention Effect for Nanomedicine Drug Delivery in Oncology. *Cancer Res.* **2013**, *73*, 2412−2417.
(53) Lammers, T.; Kiessling, F.; Hennink, W. E.; Storm, G. Drug Targeting to Tumors: Principles, Pitfalls and (Pre-) Clinical Progress. *J. Controlled Release* **2012**, *161*, 175−187.
(54) Deng, C.; Jiang, Y.; Cheng, R.; Meng, F.; Zhong, Z. Biodegradable Polymeric Micelles for Targeted and Controlled Anticancer Drug Delivery: Promises, Progress and Prospects. *Nano Today* **2012**, *7*, 467−480.
(55) Sun, W.; Lu, Y.; Gu, Z. Advances in Anticancer Protein Delivery Using Micro-/Nanoparticles. *Part. Part. Syst. Charact.* **2014**, *31*, 1204−1222.
(56) Li, X.; Yang, W.; Zou, Y.; Meng, F.; Deng, C.; Zhong, Z. Efficacious Delivery of Protein Drugs to Prostate Cancer Cells by PSMA-Targeted pH-Responsive Chimaeric Polymersomes. *J. Controlled Release* **2015**, *220*, 704−714.
(57) Jiang, T.; Sun, W.; Zhu, Q.; Burns, N. A.; Khan, S. A.; Mo, R.; Gu, Z. Furin-Mediated Sequential Delivery of Anticancer Cytokine and Small-Molecule Drug Shuttled by Graphene. *Adv. Mater.* **2015**, *27*, 1021−1028.
(58) Zhao, M.; Hu, B.; Gu, Z.; Joo, K.-I.; Wang, P.; Tang, Y. Degradable Polymeric Nanocapsule for Efficient Intracellular Delivery of a High Molecular Weight Tumor-Selective Protein Complex. *Nano Today* **2013**, *8*, 11−20.

DOI: 10.1021/acsami.6b05775
ACS Appl. Mater. Interfaces 2016, 8, 21155−21162